Supplementary Information

High saturation factor in Overhauser DNP with nitroxide derivatives: the role of ^{14}N nuclear spin relaxation

Nikolay Enkin,[a] Guoquan Liu,[a*] Maria del Carmen Gimenez-Lopez,[b] Kyriakos Porfyrakis,[c] Igor Tkach[a] and Marina Bennati[a,d*]

[a] Research Group EPR spectroscopy, Max-Planck Institute for Biophysical Chemistry, Am Fassberg 11, 37077 Göttingen, Germany.
[b] School of Chemistry, University of Nottingham, Nottingham NG7 2RD, United Kingdom.
[c] Department of Materials, University of Oxford, Oxford OX1 3PH, United Kingdom.
[d] Department of Chemistry, University of Göttingen, Tammanstr. 2, 37077 Göttingen, Germany.

SI1: Synthesis and characterization of fullerene-nitroxide (FN) derivatives

All reagents and solvents unless specified were purchased from Sigma–Aldrich and were used without further purification. NMR spectra were obtained on a Varian Mercury 300 spectrometer (300 MHz for ^{1}H). Mass spectrometry was carried out on a Bruker Ultraflex III MALDI-TOF spectrometer using DCTB as matrix (355 nm) or on a Bruker MicroTOF with electrospray ionization (ESI). UV-vis spectra were recorded at room temperature in quartz cuvettes on an Agilent Cary 100 UV-VIS spectrophotometer.

Synthesis of precursor molecules: FN and the malonate-derived compound (**1**) were synthesized as shown in Scheme **1** following experimental procedures reported elsewhere [1, 2]. **1** ESI-MS: 419.2 *m/z* $[M+H]^+$,^{1}H NMR (300 MHz, $CDCl_3$) δ/ppm 4.84 (s, 2H), 4.21 (t, 4H), 3.39 (s, 2H), 3.19 (t, 4H), 1.84 (m, 4H), 1.43 (s, 18H) . **FN** (MALDI-MS: 917.2 *m/z* $[M]^-$, UV-vis (toluene): 434 nm).

A)

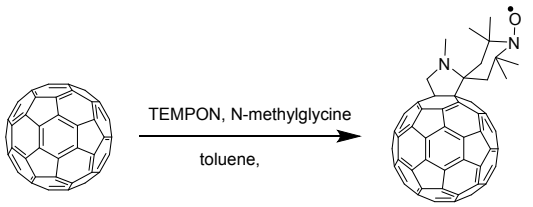

B)

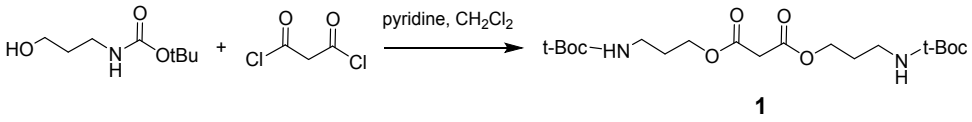

Scheme S1: Synthesis of precursors **FN** (A) and **1** (B)

Synthesis of fullerene-nitroxide derivatives: **FN-1a**, **FN-2a** and **FN-3a** were synthesized by adapting a previous report [2], in which pristine C_{60} instead of **FN** was used as building block for the synthesis of water-soluble fullerene derivatives. A modified Bingel reaction that uses mild conditions (1, 8-diazabicyclo[5.4.0]undec-7-ene and **CBr_4** as bromine source) for the *in situ* formation of α-bromomalonates was selected here to preserve the nitroxide functionality.

FN and **1** were reacted in toluene for 30-60 min in the presence of **CBr_4**, and 1,8-diazabicyclo[5.4.0]undec-7-ene (**DBU**) to obtain the target fullerene adducts using the conditions shown in **Table S1**. The desired products were purified by column chromatography (silica gel) using toluene/ethyl acetate as eluent with a yield of *c.a.* 40% for **FN-1a** (MALDI-MS: 1333.3 *m/z* $[M]^-$, UV-vis (toluene): 480 nm), *c.a.* 20% for **FN-2a** (MALDI-MS: 1749.2 *m/z* $[M]^-$, UV-vis (toluene): 472 nm) and *c.a.* 8% for **FN-3a** (MALDI-MS: 2165.2 *m/z* $[M]^-$, UV-vis (toluene): 460 nm).

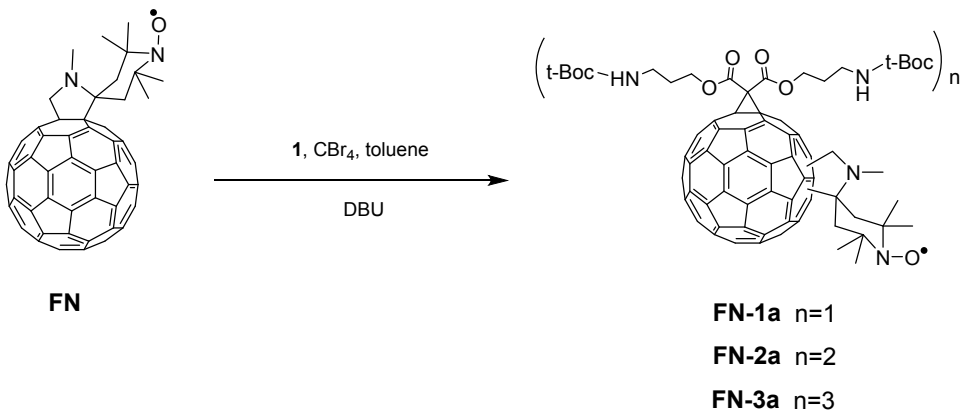

FN

FN-1a n=1
FN-2a n=2
FN-3a n=3

Scheme S2: Synthesis of fullerene-nitroxide derivatives by nucleophilic addition of the α-bromomalonate carbanion derivated to **FN** (Bingel-type reaction)

Table S1: Ratio of reactants in the synthesis of fullerene-nitroxide derivatives.

Sample	FN (equiv)	**CBr_4** (equiv)	**1** (equiv)	**DBU** (equiv)
FN-1a	1	1.5	1.5	3
FN-2a	1	2.2	2.2	4.5
FN-3a	1	3.3	3.3	6.6

Fig. S1: UV-Vis absorption spectra of fullerene-nitroxide derivatives (~ 0.1 mM) in toluene at room temperature.

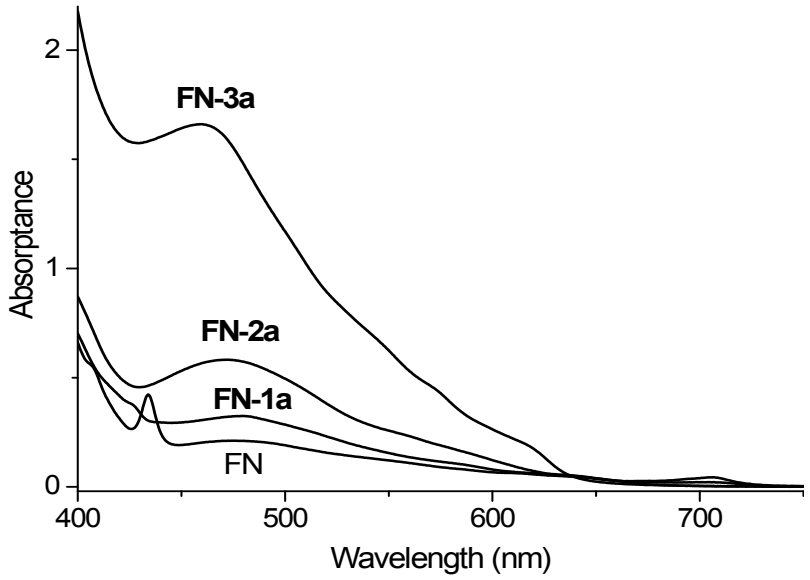

References:

1) F. Arena, F. Bullo, F. Conti, C. Corvaja, M. Maggini, M. Prato and G. Scorrano, *J. Am. Chem. Soc.*, 1997, **119**, 789-795.
2) F C. F. Richardson, D. I. Schuster and S. R. Wilson, *Org. Lett.*, 2000, **2**, 1011-1014.

Fig. S2: Normalized CW-EPR spectra of fullerene-nitroxide derivatives in toluene.

Experimental spectra (colored lines) are for c ≈ 1.5 mM degassed solutions, black solid lines are fits with "*Easyspin*" [3]. "*Easyspin*" simulation was used to determine the molecular rotational correlation time τ_c for each sample, which is reported in Table 1, main text. We note that the line widths of TL slightly exceed the ones of FN likely due to some residual oxygen content. However, the rotational correlation time of FN still results slower (0.01 ns vs. 0.06 ns for TL and FN, respectively), as picked up by the simulation and reflected in the relative intensity of the high field vs central hyperfine lines. *Exp. parameters: microwave power = 2 mW; 1 G modulation amplitude, 100 kHz modulation frequency, 1024 points/spectrum, room temperature.*

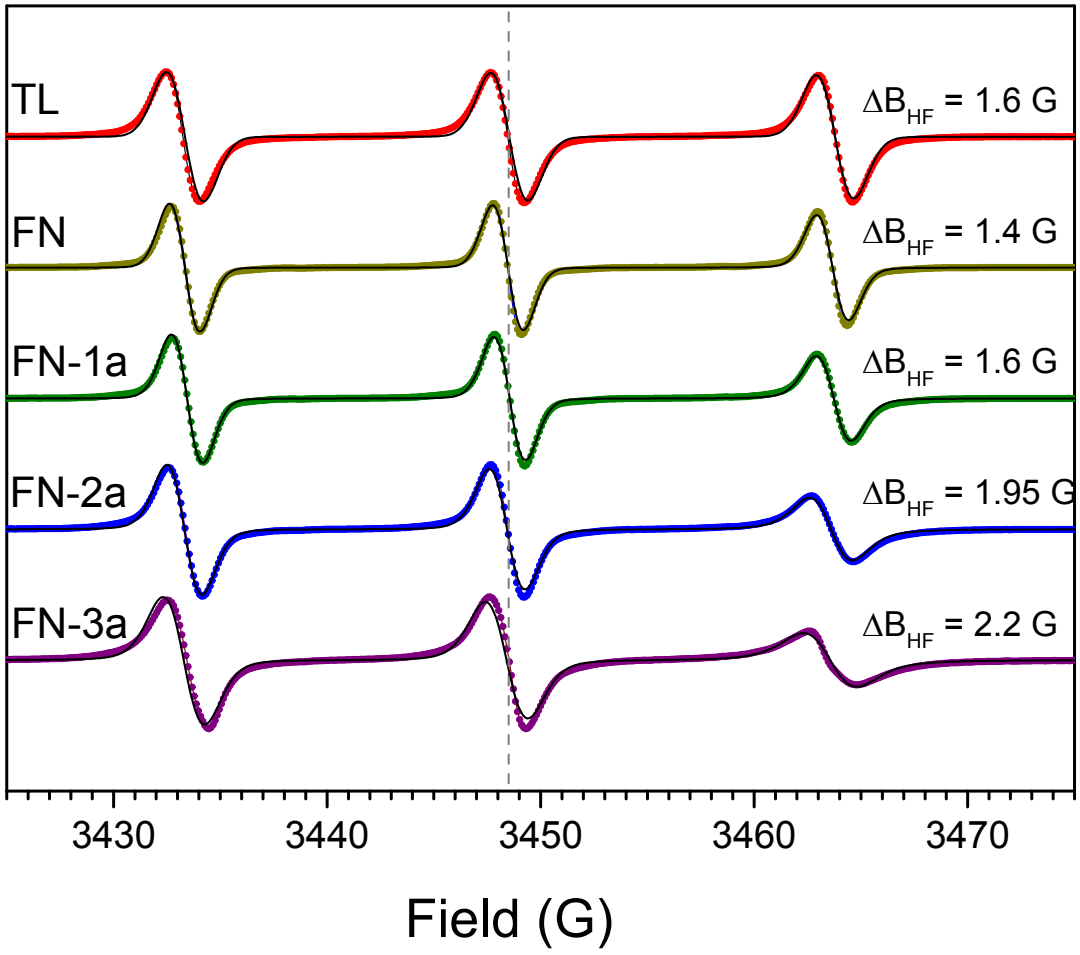

In the fast-motion regime, where the speed of rotational diffusion (τ_c^{-1}) is fast as compared to the anisotropic interactions, the Redfield theory leads to simplified expressions for EPR line widths in solution. For the case of an EPR line with hyperfine and g anisotropy, the widths of individual hyperfine lines are given by the quadratic expression [3]:

$$\Delta\nu = A_0 + A + B \cdot m_I + C \cdot m_I^2 \qquad (4)$$

where Δν is the linewidth (FWHM) of the Lorentzian line in frequency units, m_I is the nuclear magnetic quantum number of the considered hyperfine line, (A, B, C) are coefficients that characterize the averaging of the anisotropy by molecular motion. A_0 collects all other

broadening effects. With knowledge of the ***g*** and ***A*** (hyperfine) tensors, the isotropic rotational correlation time τ_c can be obtained from A, B, C according to [3]:

$$A = \frac{\mu_e^2}{h^2} B_0^2 \left(\Delta g : \Delta g\right)\left[\tfrac{2}{15} j_0 + \tfrac{1}{10} j_1\right] + I\left(I+1\right)\left(\Delta A : \Delta A\right)\left[\tfrac{2}{15} j_0 + \tfrac{7}{60} j_1\right]$$
$$B = \frac{16\pi^2}{15} \frac{\mu_e}{h} B_0 \left(\Delta g : \Delta A\right)\left[\tfrac{5}{15} j_0 + \tfrac{1}{5} j_1\right] \qquad (5)$$
$$C = \left(\Delta A : \Delta A\right)\left[\tfrac{1}{12} j_0 - \tfrac{1}{60} j_1\right]$$

with spectral densities of the form $j_0 = \tau_C$ and $j_1 = \tau_C / \left(1 + \omega_0^2 \tau_C^2\right)$. Δg and $\Delta \boldsymbol{A}$ are the anisotropic parts of the ***g*** and ***A*** tensors, i.e. $\Delta \boldsymbol{g} = \boldsymbol{g} - g_{iso}\mathbf{1}$ and $\Delta \boldsymbol{A} = \boldsymbol{A} - a_{iso}\mathbf{1}$ ($\Delta \boldsymbol{A}$ is given in frequency units, **1** is the unit matrix). The notation ***X*:*Y*** indicates element-by-element multiplication of the matrices followed by summation, giving a number characterizing the corresponding anisotropy.

References:

3) S. Stoll and A. Schweiger, Easyspin: Simulating CW ESR spectra, *ESR Spectroscopy in Membrane Biophysics*, 2007, **27**, 299-321.

SI2: Experimental setup for low-field DNP.

The low-field DNP spectrometer consists of a commercial Bruker ElexSys E500 CW EPR spectrometer equipped with a Bruker 5 W CW amplifier (AmpX) and a Bruker Minispec for NMR detection (2-60 MHz). A Bruker FlexLine dielectric microwave resonator (EN 4118X-MD-4) with matched ENDOR coils for proton NMR at 14 MHz is used for X-band (9.7 GHz) EPR and DNP. For DNP, a liquid sample is continuously irradiated for several seconds by microwave in resonance with one of the hyperfine EPR transitions and subsequently the nuclear magnetization is measured with FID detection. To avoid heating of the resonator, a constant flow of N_2 gas inside of the cavity is supplied. Other experimental details are provided in the main text.

SI3: Evaluation of DNP enhancements for ring and methyl protons in toluene.

The amplitude ratios of DNP vs Boltzmann signal were calculated for two individual peaks in the spectra and related to the DNP enhancement ε according to:

$$\varepsilon_{Ring} = \frac{I_{Ring,\,DNP}}{I_{Ring,\,Bol}} \approx \frac{\Delta\nu_{Ring,\,DNP} \cdot h_{Ring,\,DNP}}{\Delta\nu_{Ring,\,Bol} \cdot h_{Ring,\,DNP}} = k_{Ring} \cdot E_{Ring}$$
$$\varepsilon_{Methyl} = \frac{I_{Methyl,\,DNP}}{I_{Methyl,\,Bol}} \approx \frac{\Delta\nu_{Methyl,\,DNP} \cdot h_{Methyl,\,DNP}}{\Delta\nu_{Methyl,\,Bol} \cdot h_{Methyl,\,DNP}} = k_{Methyl} \cdot E_{Methyl} \quad (1)$$

where I is the area of the NMR Lorentzian line, h is the maximum of the absorption line, $\Delta\nu$ is the width at the half height, and $\boldsymbol{E = h_{DNP}/h_{Bol}}$ is the ratio of the amplitudes [4, 5]. The factor $\boldsymbol{k = \Delta\nu_{DNP}/\Delta\nu_{Bol}}$ is introduced to account for the artificial broadening observed during signal averaging. This broadening might occur due to field instability caused by the electromagnet (no shimming is available in our set up). Assuming that line broadening is of similar magnitude after the same number of accumulations, we set $\boldsymbol{k_{Ring} \approx k_{Methyl} \approx k}$. The factor k was determined for each individual sample/concentration.

The FID reflects the DNP signal enhancement ε_{FID} according to the contribution of five ring and three methyl protons:

$$\frac{5 \cdot \varepsilon_{Ring} + 3 \cdot \varepsilon_{Methyl}}{8} = \varepsilon_{FID} \quad (2)$$

With further substitution $\boldsymbol{\varepsilon_{Ring} = k \cdot E_{Ring}}$, $\boldsymbol{\varepsilon_{Methyl} = k \cdot E_{Methyl}}$ in eq. (2) we obtain:

$$\frac{k \cdot \left(5 \cdot E_{Ring} + 3 \cdot E_{Methyl}\right)}{8} = \varepsilon_{FID} \quad (3)$$

From the observed FID enhancement and the enhancement of the amplitudes E, the factor k was calculated, which was then used in eq. (1) to obtain the absolute enhancement ε_{Ring} and ε_{Methyl} of each type of protons.

References:

4) C. P. Poole, Electron Spin Resonance, John Wiley & Sons, New York, 1983, 783.
5) N. Enkin, G. Liu, I. Tkach and M. Bennati, (SI), *Phys. Chem. Chem. Phys.,* 2014, **16**, 8795.

Fig. S3: MW power dependence of the peak-to-peak intensity of the central nitroxide hyperfine line. The solid lines represent curves fitted with the function:

$$y' = y'_0 c\sqrt{QP} \Big/ (1+\gamma_s^2 T_1 T_2 c^2 QP)^{3/2} \tag{6}$$

where P is the microwave power, γ_s is the gyromagnetic ratio of the electron, T_1 and T_2 are the spin-lattice and spin-spin relaxation times, respectively, $y'_0 c\sqrt{Q}$ is the slope of the curves at low power, c^2QP is related to the microwave field strength $B_1 = c\sqrt{QP}$ ($c \cdot Q^{1/2} = (46 \pm 4) \times 10^{-3}$ $mW^{-1/2}$) [6]. Using the results of the fits, the saturation factor s_{irr} of an irradiated EPR line is calculated with:

$$s_{irr} = \gamma_s^2 T_1 T_2 c^2 QP \Big/ \left(1+\gamma_s^2 T_1 T_2 c^2 QP\right) \tag{7}$$

At a the microwave power of 3W, which is applied in our DNP experiments in the same cavity set up, the saturation factors of the fullerene-nitroxide derivatives (c ≈ 1.5 mM) is close to unity.

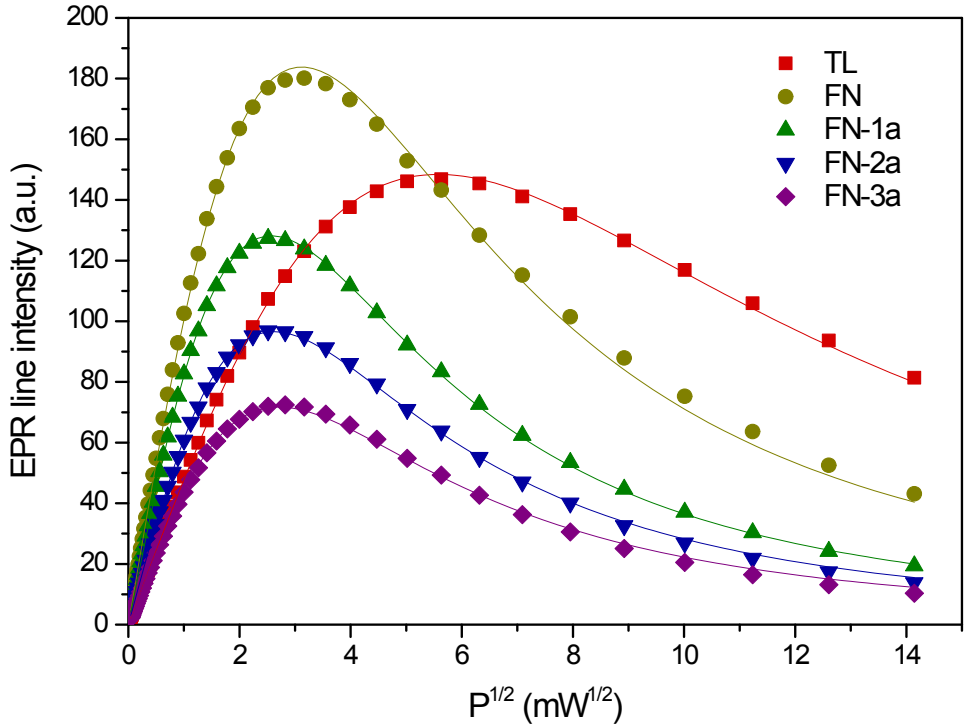

References:

6) C. P. Poole, Electron Spin Resonance, John Wiley & Sons, New York, 1983.

Fig. S4: ELDOR saturation spectra. Normalized FID intensities of **TL** (a), **FN** (b), **FN-1a** (c), **FN-2a** (d) and **FN-3a** (e), respectively, as a function of the frequency of a saturation pulse. Three consecutive experiments per sample were performed with detection on the low, central and high field hyperfine line. The obtained saturation factors of the individual lines $s_{1,2,3}$ are reported in Table S2, the resulting effective saturation factors $s_{eff} = \frac{s_1 + s_2 + s_3}{3}$ for pumping on the central line are displayed in Table 1, main text. Pulse sequence is illustrated in main text. *Exp. parameters: C = 1.5 mM; $t_{\pi/2}$ = 24 ns; t_{pump} = 1 µs; B_1 ~ 2−3 G; room temperature*.

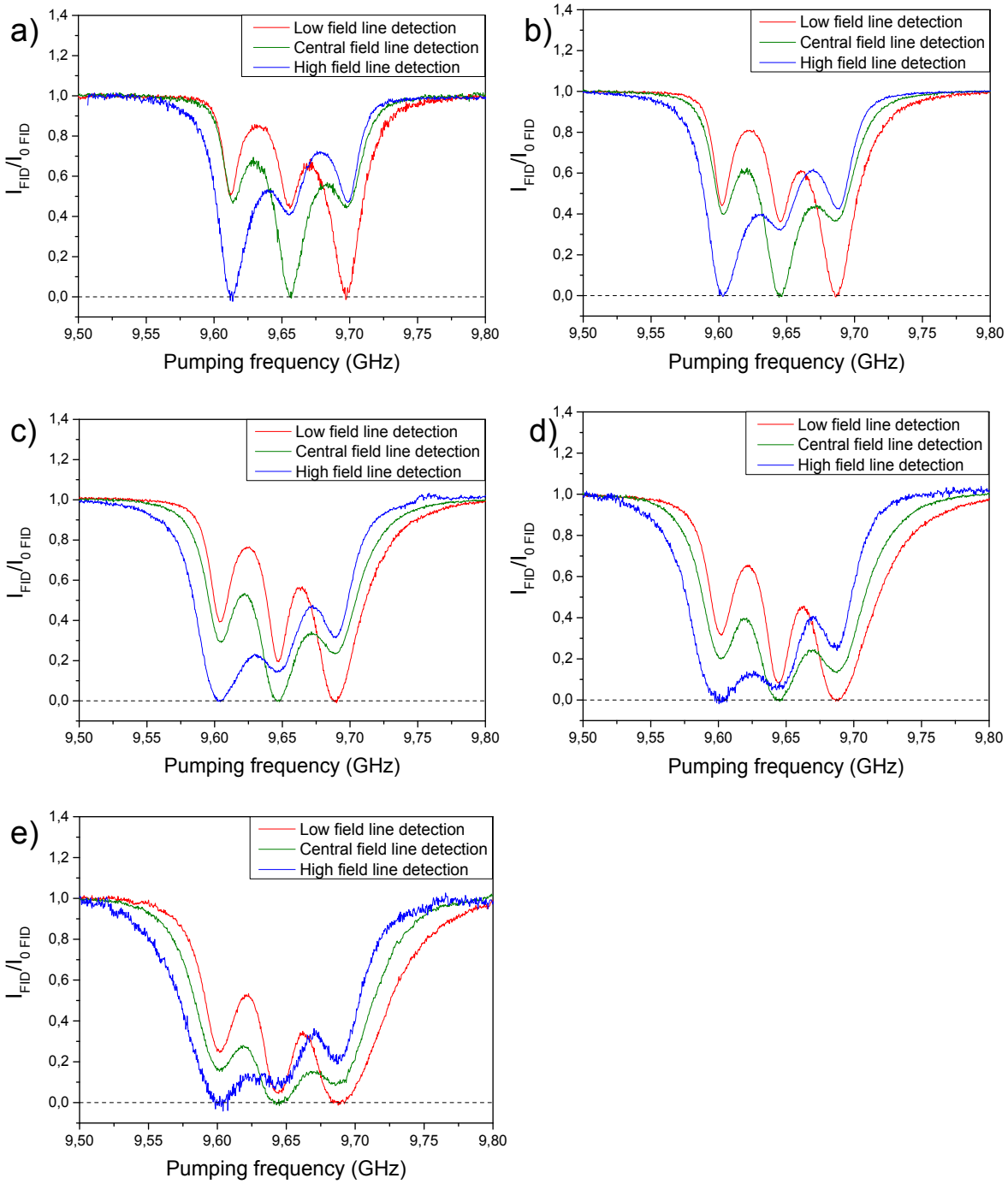

Fig. S5: Time evolution of polarization recovery (PR) EPR and ELDOR curves. The time evolution of the FID intensity was recorded after a pump pulse in resonance with the high field line and the detection pulse resonant with low (red), central (green) and high field (blue) hyperfine lines, respectively. Pumping on the high field line (the latter is weakest in intensity) allows for detection of the ELDOR effect on the neighbor lines with the highest signal intensity. Curves for **TL** (a), **FN** (b), **FN-1a** (c), **FN-2a** (d), **FN-3a** (e), were fitted with tri-exponential functions, and shared parameters within one sample, according to eq. 3 in the main text. Extracted $1/T_{1e} = 2w_e$ is reported in Table 1 (main text). Parameters $1/T_{1n} = 2w_n$ and K_x from the fits are plotted in Fig. 5 (main text) as a function of the rotational correlation time of the individual fullerene-nitroxide derivatives. *Experimental parameters: c = 1.5 mM;* $t_{\pi/2}$ *= 24 ns;* t_{pump} *= 0.1 µs;* $B_1 \sim 2-3$ *G; room temperature.*

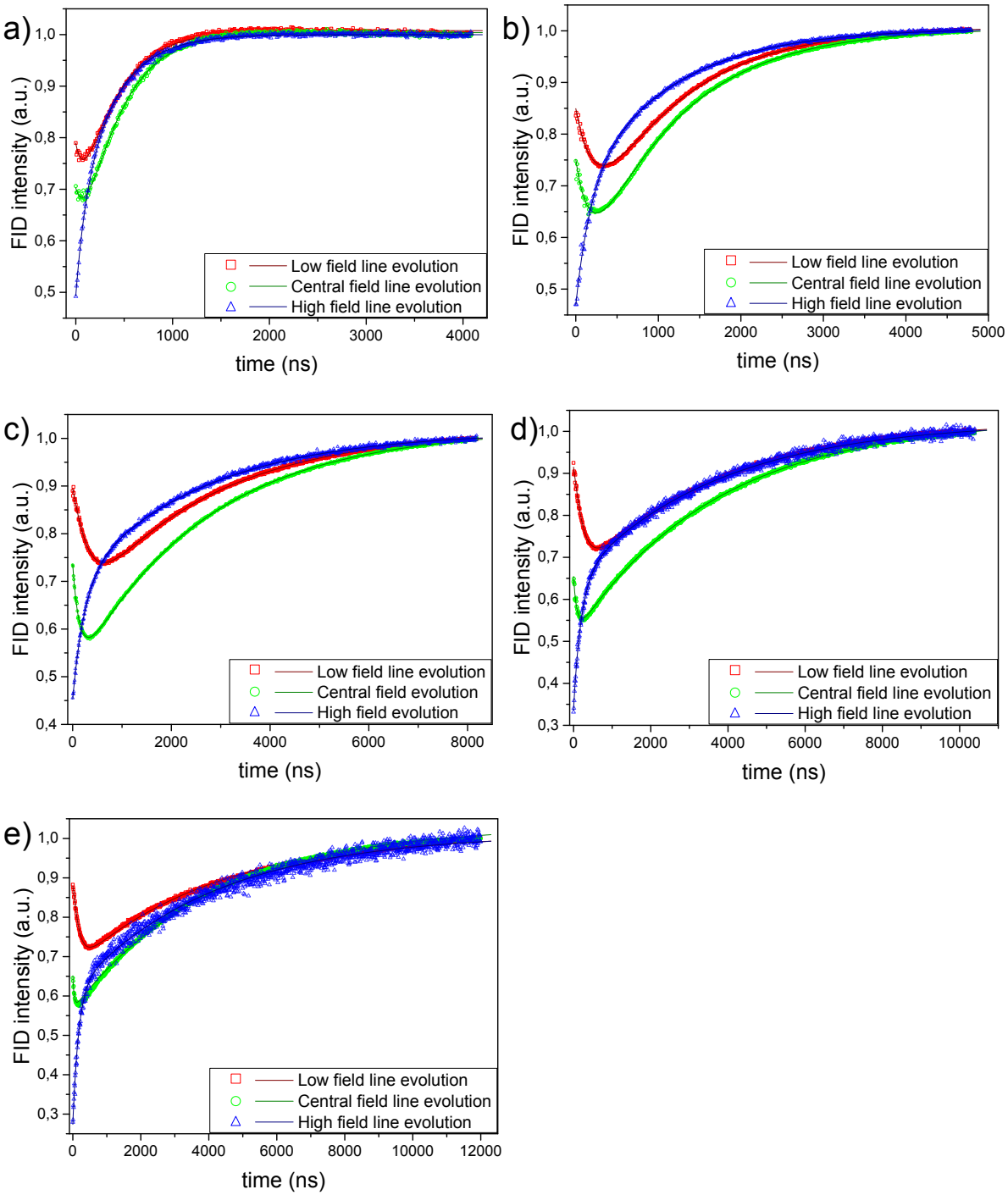

SI4: Relaxation model of a *S*=1/2, *I* =1 electron-nuclear coupled spin system and analytical expressions for the saturation factors of the individual hyperfine lines.

The time evolution of the spin populations in a nitroxide based spin system (S = ½ and I = 1) under the effect of microwave pumping on one EPR transition can be described by a combination of electron and nuclear (^{14}N) spin lattice relaxations and other relaxation mechanisms that lead to exchange of populations between the nitroxide hyperfine lines. To describe the ELDOR effect, following relaxation mechanisms could in principle lead to a coupling of the three nitroxide hyperfine lines: Heisenberg spin exchange (HE), nitrogen spin-lattice relaxation, electron-nuclear dipolar relaxation and intermolecular electron-electron dipolar relaxation. In the DNP literature, so far only HE and nitrogen spin relaxation have been discussed when using moderate polarizer concentrations (c ≤ 25 mM) [7] based on experimental observations. Competition of HE with electron-electron dipolar interaction has been previously discussed in the literature [8] and HE was found to be dominant in low-viscosity media. For these reasons, to describe electron saturation at our polarizer concentrations (c ≈ 1.5 mM) we consider here only electron and ^{14}N nuclear spin relaxations combined with HE.

In this approach, we first explicitly derive the expressions reported by Hyde et al. [9] for polarization recovery ELDOR experiments with nitroxide radicals. In a second step we extend the treatment to derive analytical expressions for the saturation factors of individual lines and thus to calculate the effective saturation for DNP. Following the initial model of Bates and Drozdoski [7], we consider the Heisenberg exchange (HE) as an intermolecular process, in which the individual ^{14}N nuclear spin states as well as the total electron spin state are conserved. In the following we define the states $|1\rangle=|+;+1\rangle$, $|2\rangle=|-;+1\rangle$, $|3\rangle=|+;0\rangle$, $|4\rangle=|-;0\rangle$, $|5\rangle=|+;-1\rangle$, $|6\rangle=|-;-1\rangle$ [9, 7], where ± denotes the m_s = ± ½ electron spin states whereas 0 and ± 1 the ^{14}N nuclear states. According to this, the HE, which is induced by a collision of two molecules with different nuclear and electron spin states, leads effectively to the following exchange of populations:

$$\begin{aligned} |1\rangle+|4\rangle &\xleftrightarrow{K_x} |2\rangle+|3\rangle \\ |3\rangle+|6\rangle &\xleftrightarrow{K_x} |4\rangle+|5\rangle \\ |1\rangle+|6\rangle &\xleftrightarrow{K_x} |2\rangle+|5\rangle \end{aligned} \quad (8)$$

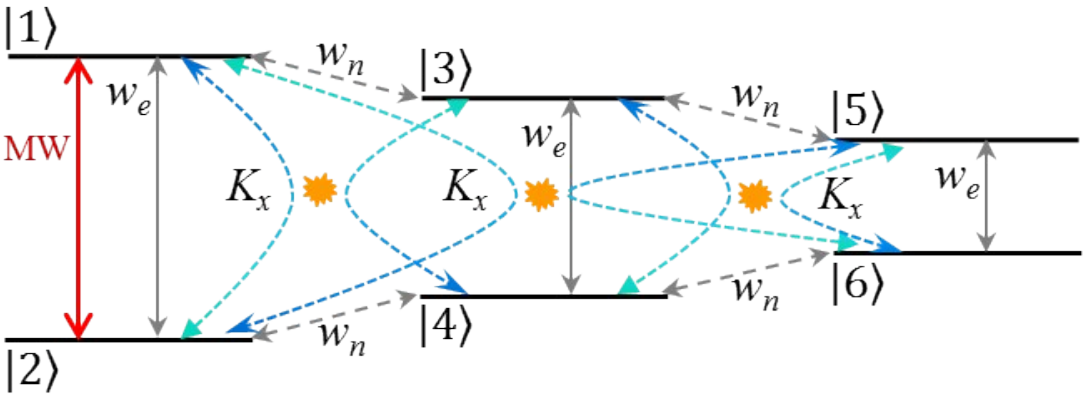

Scheme S3: Relaxation scheme for the S = ½ and I = 1 coupled spin system. The red arrow indicates a continuous MW irradiation at one of the hyperfine EPR transitions. Labelling of the spin states is according to ref. 8 and 9 for consistency with the literature. The grey solid and dashed lines indicate electron (w_e) and ^{14}N nuclear (w_n) spin relaxation pathways, respectively. The blue-cyan ones (dashed) depict the HE.

The time evolution of the six states populations N_i (i = 1,...,6) can be described by the following system of the rate equations:

$$\frac{d}{dt}\begin{pmatrix} N_1 \\ N_2 \\ N_3 \\ N_4 \\ N_5 \\ N_6 \end{pmatrix} = W_R \cdot \begin{pmatrix} N_1 - N_1^B \\ N_2 - N_2^B \\ N_3 - N_3^B \\ N_4 - N_4^B \\ N_5 - N_5^B \\ N_6 - N_6^B \end{pmatrix} + V_K = W_R \cdot \begin{pmatrix} N_1 \\ N_2 \\ N_3 \\ N_4 \\ N_5 \\ N_6 \end{pmatrix} - W_R \cdot \begin{pmatrix} N_1^B \\ N_2^B \\ N_3^B \\ N_4^B \\ N_5^B \\ N_6^B \end{pmatrix} + V_K$$

$$W_R = \begin{pmatrix} -w_e - w_n & w_e & w_n & 0 & 0 & 0 \\ w_e & -w_e - w_n & 0 & w_n & 0 & 0 \\ w_n & 0 & -w_e - 2w_n & w_e & w_n & 0 \\ 0 & w_n & w_e & -w_e - 2w_n & 0 & w_n \\ 0 & 0 & w_n & 0 & -w_e - w_n & w_e \\ 0 & 0 & 0 & w_n & w_e & -w_e - w_n \end{pmatrix}$$

$$V_K = \begin{pmatrix} -K_x N_1 N_4 + K_x N_2 N_3 - K_x N_1 N_6 + K_x N_2 N_5 \\ K_x N_1 N_4 - K_x N_2 N_3 + K_x N_1 N_6 - K_x N_2 N_5 \\ K_x N_1 N_4 - K_x N_2 N_3 - K_x N_3 N_6 + K_x N_4 N_5 \\ -K_x N_1 N_4 + K_x N_2 N_3 + K_x N_3 N_6 - K_x N_4 N_5 \\ K_x N_1 N_6 - K_x N_2 N_5 + K_x N_3 N_6 - K_x N_4 N_5 \\ -K_x N_1 N_6 + K_x N_2 N_5 - K_x N_3 N_6 + K_x N_4 N_5 \end{pmatrix} \quad (9)$$

where $2w_e$, $2w_n$ are the electron and ^{14}N nuclear relaxation rates, respectively; K_x is the normalized Heisenberg spin exchange (HE) rate per mole, which is a second order (inter-molecular) rate parameter; W_R is the relaxation matrix and V_K is a vector defined to account for the HE rate according to (8). N_i^B ($i=1...6$) correspond to the Boltzmann level populations.

The EPR signal intensity is expressed in form of population differences:

$$\begin{aligned} i_1 &= N_2 - N_1 \\ i_2 &= N_4 - N_3 \\ i_3 &= N_6 - N_5 \end{aligned} \quad (10)$$

with the conserved total population $N = N_1 + N_2 + N_3 + N_4 + N_5 + N_6 = N^B$. With the above definition of the states, the i_1 is the intensity of the low field line and i_3 is the high field line.

Likewise,

$$
\begin{aligned}
i_1^B &= N_2^B - N_1^B \\
i_2^B &= N_4^B - N_3^B \\
i_3^B &= N_6^B - N_5^B
\end{aligned}
\tag{11}
$$

where i_1^B, i_2^B, i_3^B are proportional to the EPR signals at thermal equilibrium.

To express the time dependence as a function of signal intensities, we perform a linear equation transformation and introduce following additional parameters: $i_{n12} = N_1 + N_2 - N_3 - N_4$, $i_{n12}^B = N_1^B + N_2^B - N_3^B - N_4^B$ (sum of NMR intensities from transitions between $m_I = -1$ *and* $m_I = 0$ states) and $i_{n23} = N_3 + N_4 - N_5 - N_6$, $i_{n23}{}^B = N_3^B + N_4^B - N_5^B - N_6^B$ (sum of NMR intensities from transitions between $m_I = 0$ *and* $m_I = +1$ states). After the transformation (using *Mathematica*, Wolfram Research, Inc.), the new system of the equations reduces to:

$$
\frac{d}{dt}\begin{pmatrix} N \\ i_1 \\ i_2 \\ i_3 \\ i_{n12} \\ i_{n23} \end{pmatrix} = \widetilde{W}_R \cdot \begin{pmatrix} N \\ i_1 \\ i_2 \\ i_3 \\ i_{n12} \\ i_{n23} \end{pmatrix} - \widetilde{W}_R \cdot \begin{pmatrix} N^B \\ i_1{}^B \\ i_2{}^B \\ i_3{}^B \\ i_{n12}{}^B \\ i_{n23}{}^B \end{pmatrix} + \widetilde{V}_K
$$

$$
\widetilde{W}_R = \begin{pmatrix}
0 & 0 & 0 & 0 & 0 & 0 \\
0 & -2w_e - w_n & w_n & 0 & 0 & 0 \\
0 & w_n & -2w_e - 2w_n & w_n & 0 & 0 \\
0 & 0 & w_n & -2w_e - w_n & 0 & 0 \\
0 & 0 & 0 & 0 & -2w_n & w_n \\
0 & 0 & 0 & 0 & w_n & -2w_n
\end{pmatrix}
$$

$$
\widetilde{V}_K = \begin{pmatrix}
0 \\
\frac{1}{3}K_x N(-2i_1 + i_2 + i_3) + \frac{2}{3}i_{n12}K_x(i_1 + i_2 + i_3) + \frac{1}{3}i_{n23}K_x(i_1 + i_2 + i_3) \\
\frac{1}{3}K_x N(i_1 - 2i_2 + i_3) - \frac{1}{3}i_{n12}K_x(i_1 + i_2 + i_3) + \frac{1}{3}i_{n23}K_x(i_1 + i_2 + i_3) \\
\frac{1}{3}K_x N(i_1 + i_2 - 2i_3) - \frac{1}{3}i_{n12}K_x(i_1 + i_2 + i_3) - \frac{2}{3}i_{n23}K_x(i_1 + i_2 + i_3) \\
0 \\
0
\end{pmatrix}.
\tag{12}
$$

Since the ^{14}N-NMR signal terms ($i_{n12}, i_{n23}, i_{n12}^B, i_{n23}^B$) are much smaller compared with the EPR signal (i_1, i_2, i_3) because $\omega_e >> \omega_A$ ($\omega_e/2\pi \approx 9$ GHz – electron Larmor frequency, $\omega_A/2\pi \approx 20$ MHz – splitting of ^{14}N nuclear spin including the hyperfine coupling in ^{14}NO•), all elements in $\widetilde{V}_K$ containing their products are neglected. Furthermore, the total population N is a constant value ($N^B = N$). Thus, the system of the equations simplifies to:

$$\frac{d}{dt}\begin{pmatrix} i_1 \\ i_2 \\ i_3 \end{pmatrix} = \widetilde{W}_R^* \cdot \begin{pmatrix} i_1 - i_1^B \\ i_2 - i_2^B \\ i_3 - i_3^B \end{pmatrix} + \widetilde{W}_K^* \cdot \begin{pmatrix} i_1 \\ i_2 \\ i_3 \end{pmatrix} = \left(\widetilde{W}_R^* + \widetilde{W}_K^*\right) \begin{pmatrix} i_1 - i_{1B}^* \\ i_2 - i_{2B}^* \\ i_3 - i_{3B}^* \end{pmatrix} = W \cdot \begin{pmatrix} i_1 - i_{1B}^* \\ i_2 - i_{2B}^* \\ i_3 - i_{3B}^* \end{pmatrix}$$

$$\widetilde{W}_R^* = \begin{pmatrix} -2w_e - w_n & w_n & 0 \\ w_n & -2w_e - 2w_n & w_n \\ 0 & w_n & -2w_e - w_n \end{pmatrix}, \widetilde{W}_K^* = \begin{pmatrix} -\frac{2}{3}K_x N & \frac{1}{3}K_x N & \frac{1}{3}K_x N \\ \frac{1}{3}K_x N & -\frac{2}{3}K_x N & \frac{1}{3}K_x N \\ \frac{1}{3}K_x N & \frac{1}{3}K_x N & -\frac{2}{3}K_x N \end{pmatrix}, \quad (13)$$

$$W = \widetilde{W}_R^* + \widetilde{W}_K^* = \begin{pmatrix} -2w_e - w_n - \frac{2}{3}K_x N & w_n + \frac{1}{3}K_x N & \frac{1}{3}K_x N \\ w_n + \frac{1}{3}K_x N & -2w_e - 2w_n - \frac{2}{3}K_x N & w_n + \frac{1}{3}K_x N \\ \frac{1}{3}K_x N & w_n + \frac{1}{3}K_x N & -2w_e - w_n - \frac{2}{3}K_x N \end{pmatrix}$$

$$i_{kB}^* \ (k = 1, 2, 3): \ \widetilde{W}_R^* \cdot \begin{pmatrix} i_1^B \\ i_2^B \\ i_3^B \end{pmatrix} = W \cdot \begin{pmatrix} i_{1B}^* \\ i_{2B}^* \\ i_{3B}^* \end{pmatrix}$$

The $i_{kB}^* \ (k = 1, 2, 3)$ take into account also the effect of HE, which affects the Boltzmann distribution. The rate matrix *W*, which describes the time evolution of polarization recovery, can be diagonalized leading to the real eigenvalues ($-2w_e$, $-2w_e-3w_n-K_xN$, $-2w_e-w_n-K_xN$) with different combinations of the relaxation rates and the eigenvectors ($\begin{pmatrix} 1 \\ 1 \\ 1 \end{pmatrix}, \begin{pmatrix} 1 \\ -2 \\ 1 \end{pmatrix}, \begin{pmatrix} 1 \\ 0 \\ -1 \end{pmatrix}$), respectively. The solution is then obtained as a sum of three exponential terms (*k* = *1*, *2*, *3*), consistent with the results in Ref. [8]:

$$\begin{pmatrix} i_1 \\ i_2 \\ i_3 \end{pmatrix} = A\begin{pmatrix} 1 \\ 1 \\ 1 \end{pmatrix} e^{-2w_e t} + B\begin{pmatrix} 1 \\ -2 \\ 1 \end{pmatrix} e^{-(2w_e + 3w_n + K_x N)t} + C\begin{pmatrix} 1 \\ 0 \\ -1 \end{pmatrix} e^{-(2w_e + w_n + K_x N)t} + \begin{pmatrix} i_{1B}^* \\ i_{2B}^* \\ i_{3B}^* \end{pmatrix} \quad (14)$$

Here, the parameters *A*, *B*, *C* are given by the initial conditions in each individual experiment. Therefore, for good quality of the fit one can neglect the fixed amplitude ratio of the signals obtained from the eigenvectors but just take into account their signs.

Under continuous MW irradiation in resonance with one of the EPR transitions, a steady-state of all populations with a fixed ratio of the line intensity is generated. MW affects the irradiated transition only. Analytical expressions for the saturation factors can be obtained from the kinetic equations (13) but reducing the number of variables. For instance, if the first line i_1 is irradiated, the matrix row corresponding to this variable can be removed. If the microwave power is large enough, the irradiated transition reaches a complete saturation (s_k = 1, where *k* is the number of the irradiated EPR line). Solving the equations at this condition we derive an analytical expression for the saturation of the other two EPR transitions:

$$\frac{d}{dt}\begin{pmatrix} i_2 \\ i_3 \end{pmatrix} = \begin{pmatrix} 0 \\ 0 \end{pmatrix} = \begin{pmatrix} w_n + \frac{1}{3}K_x N & -2w_e - 2w_n - \frac{2}{3}K_x N & w_n + \frac{1}{3}K_x N \\ \frac{1}{3}K_x N & w_n + \frac{1}{3}K_x N & -2w_e - w_n - \frac{2}{3}K_x N \end{pmatrix} \begin{pmatrix} i_1^s - i_{1B}^* \\ i_2^s - i_{2B}^* \\ i_3^s - i_{3B}^* \end{pmatrix} \quad (15)$$

where i_k^s (k = *1*, *2*, *3*) are the steady-state signal intensities of the EPR lines. After introducing the saturation factor $s_k = \frac{i_{kB}^* - i_k^s}{i_{kB}^*}$ ($i_{1B}^* = i_{2B}^* = i_{3B}^* = i_B^*$):

$$\begin{pmatrix} i_B^* \\ 0 \\ 0 \end{pmatrix} = \begin{pmatrix} 1 & 0 & 0 \\ w_n + \frac{1}{3}K_x N & -2w_e - 2w_n - \frac{2}{3}K_x N & w_n + \frac{1}{3}K_x N \\ \frac{1}{3}K_x N & w_n + \frac{1}{3}K_x N & -2w_e - w_n - \frac{2}{3}K_x N \end{pmatrix} \begin{pmatrix} s_1 \cdot i_B^* \\ s_2 \cdot i_B^* \\ s_3 \cdot i_B^* \end{pmatrix} \quad (16)$$

The corresponding expressions for s_2 and s_3 are:

$$s_2 = 1 - \frac{1}{1 + \frac{w_n + \frac{1}{3}K_x N + \frac{1}{6w_e}(3w_n + K_x N)(w_n + K_x N)}{2w_e + 2w_n + K_x N}}$$

$$s_3 = 1 - \frac{1}{1 + \frac{\frac{1}{3}K_x N + \frac{1}{6w_e}(3w_n + K_x N)(w_n + K_x N)}{2w_e + 3w_n + K_x N}}, \quad (17)$$

While, in the case of complete saturation of the central line (s_2 = *1*):

$$\begin{pmatrix} 0 \\ 0 \end{pmatrix} = \begin{pmatrix} -2w_e - w_n - \frac{2}{3}K_x N & w_n + \frac{1}{3}K_x N & \frac{1}{3}K_x N \\ \frac{1}{3}K_x N & w_n + \frac{1}{3}K_x N & -2w_e - w_n - \frac{2}{3}K_x N \end{pmatrix} \begin{pmatrix} i_1^s - i_{1B}^* \\ i_2^s - i_{2B}^* \\ i_3^s - i_{3B}^* \end{pmatrix}$$

$$\begin{pmatrix} 0 \\ i_B^* \\ 0 \end{pmatrix} = \begin{pmatrix} -2w_e - w_n - \frac{2}{3}K_x N & w_n + \frac{1}{3}K_x N & \frac{1}{3}K_x N \\ 0 & 1 & 0 \\ \frac{1}{3}K_x N & w_n + \frac{1}{3}K_x N & -2w_e - w_n - \frac{2}{3}K_x N \end{pmatrix} \begin{pmatrix} s_1 \cdot i_B^* \\ s_2 \cdot i_B^* \\ s_3 \cdot i_B^* \end{pmatrix} \quad (18)$$

The expressions for s_1 and s_3 are:

$$s_1 = s_3 = 1 - \frac{1}{1 + \frac{1}{6w_e}(3w_n + K_x N)}, \quad (19)$$

The behaviour of the system with the 3rd completely saturated line ($s_3 = 1$) is described by the same equations as with those for the first case (i.e. $s_1 = 1$) but numbering is swapped respectively. The saturation factors obtained from this calculation were compared with those extracted from the ELDOR data (Table S2) and show good agreement within an experimental error of 10-15%.

Table S2: Comparison of the saturation factors determined experimentally from ELDOR saturation spectra (see **Fig.S4**) with those, which were calculated using the analytical expressions (17-19) from **SI4** and the rate parameters (w_e, w_n and K_xN) obtained from the fitting of polarization recovery curves (PR-EPR/PR-ELDOR; **Fig.S5**). The data for the pumping on the central line are reported also in the main text.

Sample	LF line irradiation					
	s_2^{exp}	s_2^{theory}	s_3^{exp}	s_3^{theory}	s^{exp}	s^{theory}
TL	0.55	0.51	0.53	0.51	0.69	0.67
FN	0.63	0.62	0.57	0.61	0.74	0.74
FN-1a	0.76	0.81	0.68	0.76	0.82	0.85
FN-2a	0.86	0.89	0.74	0.84	0.87	0.91
FN-3a	0.91	0.92	0.79	0.89	0.90	0.94

Sample	Central line irradiation				
	s_1^{exp}	s_1^{exp}	$s_{1,3}^{theory}$	s^{exp}	s^{theory}
TL	0.55	0.59	0.51	0.71	0.68
FN	0.64	0.68	0.62	0.77	0.75
FN-1a	0.80	0.85	0.85	0.89	0.90
FN-2a	0.92	0.94	0.93	0.95	0.95
FN-3a	0.95	0.91	0.96	0.95	0.97

Sample	HF line irradiation					
	s_1^{exp}	s_1^{theory}	s_2^{exp}	s_2^{theory}	s^{exp}	s^{theory}
TL	0.49	0.51	0.53	0.51	0.67	0.67
FN	0.56	0.61	0.60	0.62	0.72	0.74
FN-1a	0.61	0.76	0.71	0.81	0.77	0.85
FN-2a	0.68	0.84	0.80	0.89	0.83	0.91
FN-3a	0.75	0.89	0.84	0.92	0.86	0.94

References:

7) R. D. Bates and W. S. Drozdoski, *J. Chem. Phys*., 1977, **67**, 4038-4044.
8) B. Berner and D. Kivelson, *J. Phys. Chem*., 1979, **83**, 1406-1412.
9) J. J. Yin, M. Pasenkiewicz-Gierula and J. S. Hyde, *P.N.A.S.*, 1987, **84**, 964-968.

Fig. S6: Dependence of the ^{14}N nuclear spin relaxation on rotational correlation time. Comparison of nitrogen nuclear spin relaxation rates from ELDOR recovery curves with calculated rates based on electron-nuclear dipolar relaxation as given by Solomon, Phys. Rev. Vol 99, p.559, 1955. The contribution from the spectral density at $J(\omega_n)$ is shown separately in the figure at the bottom. ω_e is the electron Larmor frequency at a field of 0.34 Tesla, and the nuclear energy splitting is dominated by hyperfine coupling and given in this case by ω_n=a_{iso}/2 (a_{iso} is the averaged ^{14}N hyperfine coupling in frequency units). The two data points at τ_c < 0.1 ns are upper limits. The observed behavior is similar to the one reported by B. H. Robinson et al., Science, 1994, **263**, 490-493.